Impact of Materials versus Geometric Parameters on the Contact Resistance in Organic Thin-Film Transistors

*Manfred Gruber, Egbert Zojer, Ferdinand Schürrer, and Karin Zojer**

The contact resistance is known to severely hamper the performance of organic thin-film transistors, especially when dealing with large injection barriers, high mobility organic semiconductors, or short channel lengths. Here, the relative significance of how it is affected by materials-parameters (mobility and interfacial level-offsets) and geometric factors (bottom-contact vs top-contact geometries) is assessed. This is done using drift-diffusion-based simulations on idealized device structures aiming at a characterization of the "intrinsic" situation in the absence of traps, differences in the film morphology, or metal-atoms diffusing into the organic semiconductor. It is found that, in contrast to common wisdom, in such a situation the top-contact devices do not always outperform the bottom-contact ones. In fact, the observed ratio between the contact resistances of the two device structures changes by up to two orders of magnitude depending on the assumed materials parameters. The contact resistance is also shown to be strongly dependent on the hole mobility in the organic semiconductor and influenced by the chosen point of operation of the device.

1. Introduction

Organic thin-film transistors (OTFTs) represent an excellent example which illustrates that the operation of organic electronic devices is not straight-forwardly governed by the properties of the active materials alone. Rather, the geometry of the device, i.e., the channel length,[1–3] the layer thicknesses,[4,5] the position of interlayers,[5–7] as well as the size and arrangement of the electrodes with respect to the semiconductor[8,9] are vital to achieving the desired performance.

In fact, with increasing electron and hole mobilities of the active materials,[10,11] the contact resistance, R_C, becomes an increasingly determining loss factor. While self-assembled monolayers represent a successful route to modify the injecting contacts in a bottom-contact geometry,[8,12,13] the injection via top-contacts has been modified by doping[7,14] or interlayers.[15,16] Beyond that, it has been demonstrated that the contact resistance is not only determined by the height of the injection barrier between the electrode metal and the organic semiconductor,[17,18] but also depends on the position[4,8,17,19–23] and extension[17,24] of the injecting contacts, i.e., staggered OTFTs (top-contact-bottom-gate or bottom-contact top-gate) possess contact resistances R_C that are often orders of magnitude lower than in their coplanar counterparts (bottom-contact bottom-gate) fabricated from the same material.

The origin of this profound discrepancy in R_C is still subject to debate. With the help of simulations Tessler et al.,[17] Hill,[20] Wang et al.,[23] and Gundlach et al.[21] argue that the arrangement of the electrodes in staggered devices results in an intrinsically smaller R_C than in coplanar ones for purely geometric reasons. In contrast, several extrinsic effects were identified that yield the same situation: Clusters of evaporated metal interpenetrating the semiconductor reduce R_C in staggered top-contact devices,[25,26] while the large R_C in coplanar bottom-contact devices may occur due to the presence of low mobility regions in the contact areas and traps in the contact region.[3,27,28] Beyond that, in recent simulations Brondijk et al. showed that the performance of top- vs bottom-contact devices is significantly affected by the gate voltage.[29]

It is the aim of this work to shed further light on the actual role of the device geometry and to assess its relative significance compared to materials properties, such as carrier mobilities and charge-injection barriers. Using a drift-diffusion based approach we do this avoiding effects like diffusing metal atoms, morphological inhomogeneities caused by different film growth on the electrodes and the dielectric, trap-states at the interfaces, and the field or carrier-density dependence of the mobility. Many of these effects can be readily integrated in our device model and we found the latter two essential for getting fully quantitative agreement with experimental data (including hysteresis effects), but not for explaining the then investigated general trends.[5,30] Thus, we here focus on the most fundamental processes at the contacts which allows us to extract and, importantly, also to explain the intrinsic properties of the charge-injecting contacts. To do so, we rely on our previous study of top-contact OTFT architectures in which we discussed the occurrence of different injection mechanisms as a function of the charge-injection barrier.[31] Furthermore, we do this avoiding a huge number of additional parameters necessary to account for the above-mentioned "extrinsic" effects, as these

Dr. M. Gruber, Prof. F. Schürrer, Dr. K. Zojer
Institute of Theoretical and Computational Physics
Graz University of Technology
Petersgasse 16, Graz, 8010, Austria
E-mail: karin.zojer@tugraz.at
Prof. E. Zojer
Institute of Solid State Physics
Graz University of Technology
Petersgasse 16, Graz, 8010, Austria

DOI:10. 1002/adfm.201203250

© 2013 WILEY-VCH Verlag GmbH & Co. KGaA, Weinheim

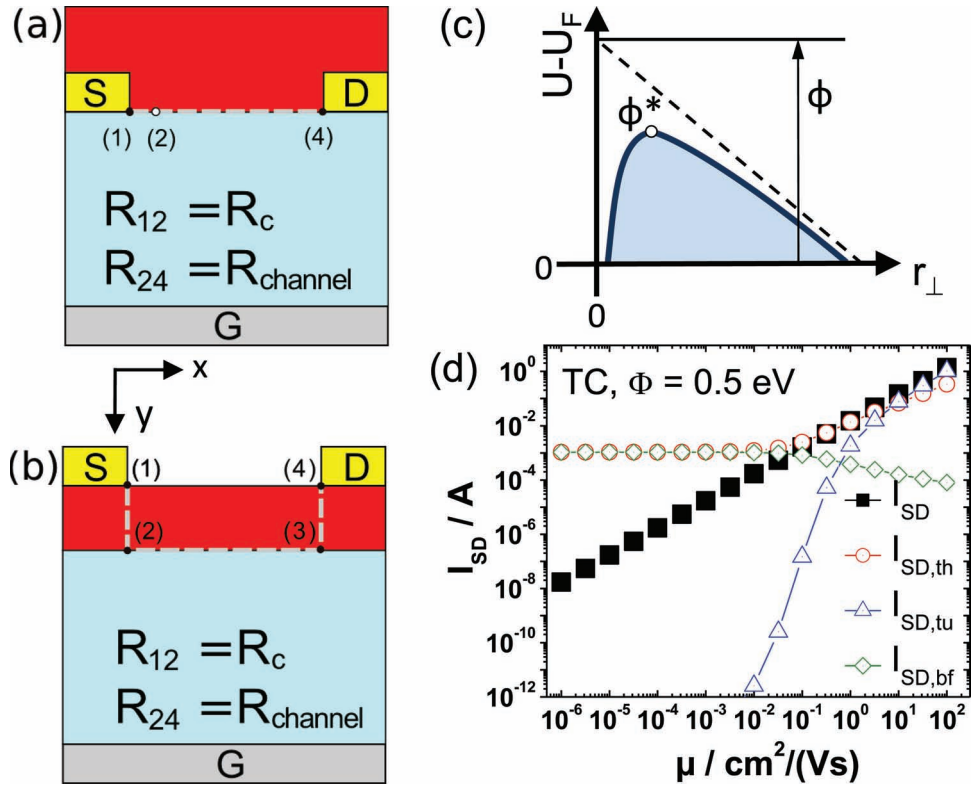

Figure 1. Schematic cross-section of a bottom-gate organic thin film transistor with bottom contacts (a) and top contacts (b). The dashed line indicates the path along which the potential distributions will be discussed in the following. Particularly relevant positions in the cross-section are labeled. c) Shape of the injection barrier (solid line) under the combined influence of an external electric field (giving rise to the potential indicated by the dashed line) and the Coulombic attraction between the injected charge and its image in the electrode. The maximum of the solid curve defines the effective barrier height, Φ^*, that is always considerably smaller than the nominal injection barrier height, Φ. d) Source-drain current, I_{SD}, and contributions due to thermionic injection $I_{SD,th}$, tunneling $I_{SD,tu}$, and back-flowing charges $I_{SD,bf}$ in a top-contact transistor (for dimensions see text) for an injection barrier of $\Phi = 0.5$ eV as a function of the mobility in the semiconductor, μ, for a device operated at $V_{DS} = -20$ V and $V_{GS} = -40$ V.

would primarily blur the obtained general picture. Building on the understanding achieved in the present study, a careful assessment of the role of the aforementioned "extrinsic" deviations from ideality will become possible in the future. Here it should be mentioned that the interplay of mobility models and contact effects (albeit as suggested in ref. [29] in the absence of the crucial barrier-shaping fields) has already been described in detail in ref. [24,32].

In passing we note that having access to carrier and field distributions within the device, we can also avoid applying the transfer (respectively, transmission)-line method frequently used both in experimental and theoretical studies. There the contact resistance is determined from the dependence of the total resistance of the device on the channel length[14,19,21,33] but the transmission-line method has been shown to fail qualitatively for a number of situations.[4,31,34]

In the following, we will focus on two possible electrode arrangements, namely bottom contact, BC, and top contact, TC, bottom-gate structures as schematically shown in **Figure 1** a,b. Charge injection and the resulting contact resistance will be described as a function of the height of the nominal injection barrier at the contact between the electrode and the organic semiconductor, Φ, and depending on the charge-carrier mobility within the organic semiconductor, μ. We find that the intrinsic contact resistance is by no means always larger for bottom-contact devices. In fact, the ratio of the contact resistances between the two studied geometries changes by several orders of magnitude over the studied parameter range and is also influenced by the operation conditions.

2. Modeling Carrier Injection and Extracting the Contact Resistance

2.1. Shape of the Injection Barrier and Injection Mechanisms

As present analytical models[4,14,23,28] do not allow to directly investigate the influence of the injection barrier on the contact resistance, we employ a simulation tool[31] based on a 2D drift-diffusion model where carrier injection at the contacts is explicitly considered.

To incorporate injection, it is convenient to describe the position within the semiconductor relative to the contour of the metal-organic interface. This is done by partitioning the position vector r, into a component $r_{\parallel}$ oriented along the interface contour, and a component $r_{\perp}$ oriented normal to it (with $r_{\perp} = 0$

© 2013 WILEY-VCH Verlag GmbH & Co. KGaA, Weinheim

corresponding to the interface). The essential quantity linking the actually injected current to the nominal injection barrier Φ (defined as the energy difference between the hole transport level and the chemical potential of the electrode) is the shape of the Schottky barrier $U(r) = U(r_{\parallel}, r_{\perp})$ at the interface[35,36]

$$U(r) = \Phi - \left(\frac{q^2}{16\pi\varepsilon_0\,\varepsilon_r(r)r_{\perp}}\right) - q\,E_{\perp}(r_{\parallel}, r_{\perp} = 0)r_{\perp} \quad (1)$$

where $q > 0$ denotes the elementary charge, ε_0 the vacuum permittivity, and $\varepsilon_r(r)$ the relative static permittivity of the semiconductor. As indicated in Figure 1c, the expression contains the combined influence of i) the nominal hole injection barrier Φ, ii) the external electric field component $E_{\perp}$ normal to the contact interface directly at the surface of the contact ($r_{\perp} = 0$) that depends on the position at the electrode surface, $r_{\parallel}$, and iii) the Coulombic attraction between the injected charge and the polarization cloud in the electrode. The inclusion of the latter two is absolutely crucial, as otherwise, qualitatively wrong trends are obtained as has been shown in ref. [29]. Point (ii) is a consequence of the externally applied drain-source- and gate-source voltages, V_{DS} and V_{GS}. Due to the absence of a high carrier concentration in the immediate vicinity of the electrodes a constant field with respect to $r_{\perp}$ is assumed for (ii). For the polarity of the electric field appropriate for carrier injection (i.e., when $E_{\perp}(r)$ is positive), $U(r)$ possesses a well-defined maximum Φ^*, denoted as the effective barrier height,[35,37] which is given by

$$\Phi^*(r_{\parallel}) = \Phi - \sqrt{\frac{q^3\,E_{\perp}(r_{\parallel}, r_{\perp} = 0)}{4\pi\,\varepsilon_0\varepsilon_r(r_{\parallel})}} \quad (2)$$

Carriers are injected across the barrier either through thermionic emission or by tunneling. For the former mechanism, the resulting current density j_{th} in the $r_{\perp}$-direction is given by the Richardson-Dushman equation and decreases exponentially with Φ^*.[36] The current density j_{tu} due to tunneling depends on the barrier-shaping field $E_{\perp}$ in a relatively complex way; here, the related transmission integral through the barrier $U(r)$ (Equation (1)) is expressed in the Wentzel-Kramers-Brillouin (WKB) approximation. To obtain a realistic description of the contact properties, one also needs to include the current density describing the back-flow of charge carriers from the semiconductor to the electrode, j_{bf}, that is a superposition of an interface-recombination current density describing the recombination of holes from the semiconductor with electrons from the metal and, when $E_{\perp}(r)$ drives carriers towards the contact, also a back-drift current density.[37] Further details regarding the mathematical treatment of the various injection processes can be found in the Methods section as well as in ref. [31,37].

The system of equations containing the Poisson, drift-diffusion current density, and continuity equations is solved self-consistently with the appropriate boundary conditions including the above described in- and out-going current densities at the source and drain electrode-semiconductor interfaces. The lateral extension of the source and drain contacts are chosen such that the steady state currents and potentials do not change with further enlarging the contacts.

2.2. Determining the Totally Injected Current and the Contact Resistance

The total injected current corresponds to the source-drain current in the transistor, I_{SD}. It can be obtained by integrating the net current density $j_{inj}(r_{\parallel})$ perpendicular to the electrode surface along the whole source electrode/semiconductor interface multiplied with the width W of the transistor

$$I_{SD} = W\int j_{inj}(r_{\parallel})\mathrm{d}r_{\parallel} = W\int [j_{th}(r_{\parallel}) + j_{tu}(r_{\parallel}) - j_{bf}(r_{\parallel})]\mathrm{d}r_{\parallel} \quad (3)$$

It equals the current at the channel entrance (2) in Figure 1a,b.[38] Formally, it can be decomposed into its individual contributions

$$I_{SD} = I_{th} + I_{tu} - I_{bf} \quad (4)$$

The inclusion of all these currents is absolutely crucial for obtaining a comprehensive picture of the device performance, as is shown in Figure 1d for the exemplary case of a TC transistor at $\Phi = 0.5$ eV considering the range of mobilities discussed below. Noteworthy, for small mobilities essentially all the thermionically injected carriers flow from the semiconductor back to the contact rather than to the channel and for large mobilities and (as shown later) also for large barriers tunneling injection becomes the dominant injection process.

The total resistance of the device R_{tot} is given by V_{DS}/I_{SD}. It can be formally split into contributions from a channel resistance, R_{ch}, and a contact resistance, R_C. The latter results from the source contact region. The drain-contact is not considered separately, as due to the forward-biasing of the corresponding Schottky diode, there is no extraction barrier for the holes and essentially no contact-induced voltage drop at the drain,[39] as also found in scanning Kelvin probe measurements.[40] To evaluate the two parts of the total resistance, it is necessary to determine, how much of the applied voltage V_{DS} drops over the source contact region (between (1) and (2) in Figure 1a,b), denoted as V_C, and how much drops over the channel (between positions (2) and (4)), referred to as V_{ch}. For determining V_C, it needs to be considered that in bottom-contact devices the potential drop in the x-direction due to the contact resistance extends over a few (ten) nanometers away from the ends of the electrode. This is interpreted as an injection distance, d_c, which defines the position of the channel entrance (2) in the BC device.[41] Details of the determination of V_C and d_C are described in the Methods Section.

3. Considered Materials Parameters, Device Dimensions, and Operation Conditions

The reference device considered in the following corresponds to a pentacene ($\varepsilon_{osc} = 3.4$)/SiO_2 ($\varepsilon_{SiO_2} = 3.9$) OTFT with a channel length of 5 μm, a channel width of 7 mm, an oxide thickness of 147 nm, a contact height of 10 nm, and a semiconductor thickness of 30 nm below (or above) the source and drain contacts (resulting in a 40 nm overall thickness for the bottom-contact device, see Figure 1). The typical hole mobility was set to μ = 1 $cm^2\ V^{-1}\ s^{-1}$ and the density of states in the active material

© 2013 WILEY-VCH Verlag GmbH & Co. KGaA, Weinheim

close to the contacts entering into the interface recombination current is set to 3×10^{27} m^{-3} in analogy to ref. [37].

Deviating from that reference device to test the impact of materials parameters, we varied the hole mobility between 1×10^{-4} cm^2 V^{-1} s^{-1} and 1×10^{2} cm^2 V^{-1} s^{-1} to cover the range found for mediocre conjugated polymers and exceeding the best single-crystal devices.[11] Further, we considered injection barriers between $\Phi = 0.0$ eV and 0.8 eV to ensure that the reported values of the prominent material combination Au/pentacene ranging from $\Phi = 0.47$ eV,[42] 0.5 eV[43,44] to 0.8 eV[45] are covered and also the value for the of Au/poly(3-hexylthiophene) (P3HT) with $\Phi \leq 0.1$ eV are included.[40,46] In contrast to ref. [31], we only consider device operation at $T = 300$ K.

Unless otherwise stated, we consider transistor operation at fixed external V_{DS} and V_{GS} in the linear regime, i.e., $|V_{GS}-V_{th}| > |V_{DS}|$. Note that the threshold voltage, V_{th}, defined as the flat-band voltage in the spirit of Meijer et al.[47] is exactly zero here due to the absence of interface charges. As typical operation conditions for conventional organic transistors we set V_{DS} = –20 V and V_{GS} = –40 V. In Section 4.2, we also discuss the dependence of R_C on the applied bias voltages.

4. Dependence of the Contact Resistance on the Injection Barrier

4.1. The Contact Resistance in the Linear Regime

In **Figure 2**a, the dependence of the contact resistance R_C on Φ is compared for top- and bottom-contact devices. As expected, for both device geometries there is an approximately exponential dependence of the contact resistance on the injection barrier, as can be inferred from the close to linear increase of R_C in the semi-logarithmic plot. Figure 2, however, also reveals a clearly different evolution for top- and bottom-contact devices, as is best seen for the ratio between $R_{C,TC}$ and $R_{C,BC}$ plotted in Figure 2b. For small injection barriers, the contact resistances for the BC devices are markedly smaller than for their TC counterparts. At intermediate injection-barriers (i.e., from $\Phi \approx 0.2$ eV to $\Phi \approx 0.5$ eV) the values for the two device geometries are rather similar, i.e., the contact resistance for one of the geometries is at the most by 50% larger than for the other geometry (dotted lines in Figure 2b). The situation changes entirely for larger barriers with the ratio of the contact resistances reaching a value of 27 for $\Phi =$ 0.8 eV. Thus, for the idealized device considered here, where extrinsic effects (see Introduction) are excluded, $R_{C,TC}/R_{C,BC}$ changes by two orders of magnitude for the considered range of nominal injection barriers.

In this context it is worth mentioning that such a trend is not necessarily always observed in modeling studies because i) it is only recovered when accounting for mirror charge effects, ii) it is influenced by the point of operation (see Section 4.2),[29] and iii) as discussed below, it is impacted also by the inclusion of tunneling injection. Moreover, extracting the contact resistance using the transfer-line method as frequently done in the literature is somewhat problematic.[31] Indeed, our data are at variance with Hill,[20] who found the relation $R_{C,BC}>R_{C,TC}$ also for barriers $\Phi < 0.3$ eV and who has been quoted for demonstrating that $R_{C,TC}$ is intrinsically smaller than $R_{C,BC}$.[48]

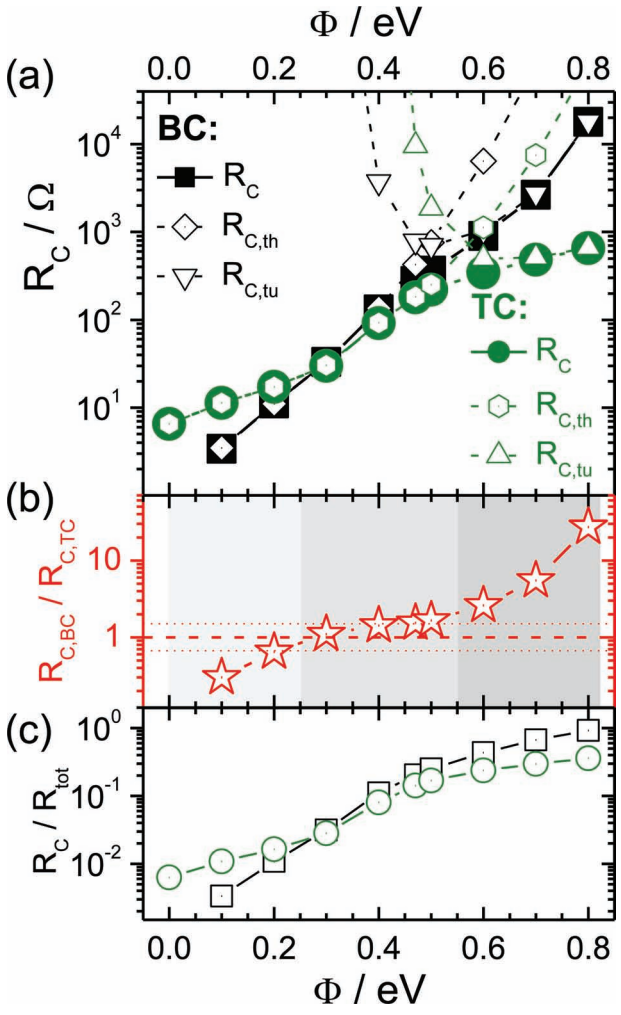

Figure 2. a) Contact resistances, R_C, of the injecting source contacts for top- (TC; green filled circles) and bottom-contact (BC; black filled squares) devices operated in the linear regime (V_{DS} = –20 V and V_{GS} = –40 V) as a function of the nominal injection barrier height Φ, assuming a hole mobility of 1 cm^2 V^{-1} s^{-1} and choosing the transistor dimensions as described in Section 3. The R_C value for $\Phi = 0$ for the BC device is vanishingly small and, thus, cannot be displayed on a logarithmic scale. Contributions of the thermionic-injection resistance, $R_{C,th}$ (open down and upward pointing triangles), and the tunneling resistance, $R_{C,tu}$ (open diamonds and open hexagons), to the total contact resistance are also shown. b) Ratio between the contact-resistances for top- and bottom-contact devices. The dashed horizontal line indicates equal contact resistances for both geometries and the dotted lines refer to ratios of 3/2 and 2/3. The shaded areas designate different injection regimes. c) Ratio between the contact-resistances and the total resistances for the top- (open green circles) and bottom-contact devices (open black squares). A table containing all values for the contact-, channel-, and total resistances can be found in the Supporting Information.

To understand to what extent the device behavior is impacted by the contact resistance, the ratio between R_C and R_{tot} is plotted in Figure 2c. One sees that the contact resistance is negligible for small barriers, its contribution to R_{tot} reaches ≈10% around $\Phi = 0.4$ eV and it becomes significant for larger barriers. Interestingly, while the maximum contribution of R_C to R_{tot} remains

© 2013 WILEY-VCH Verlag GmbH & Co. KGaA, Weinheim

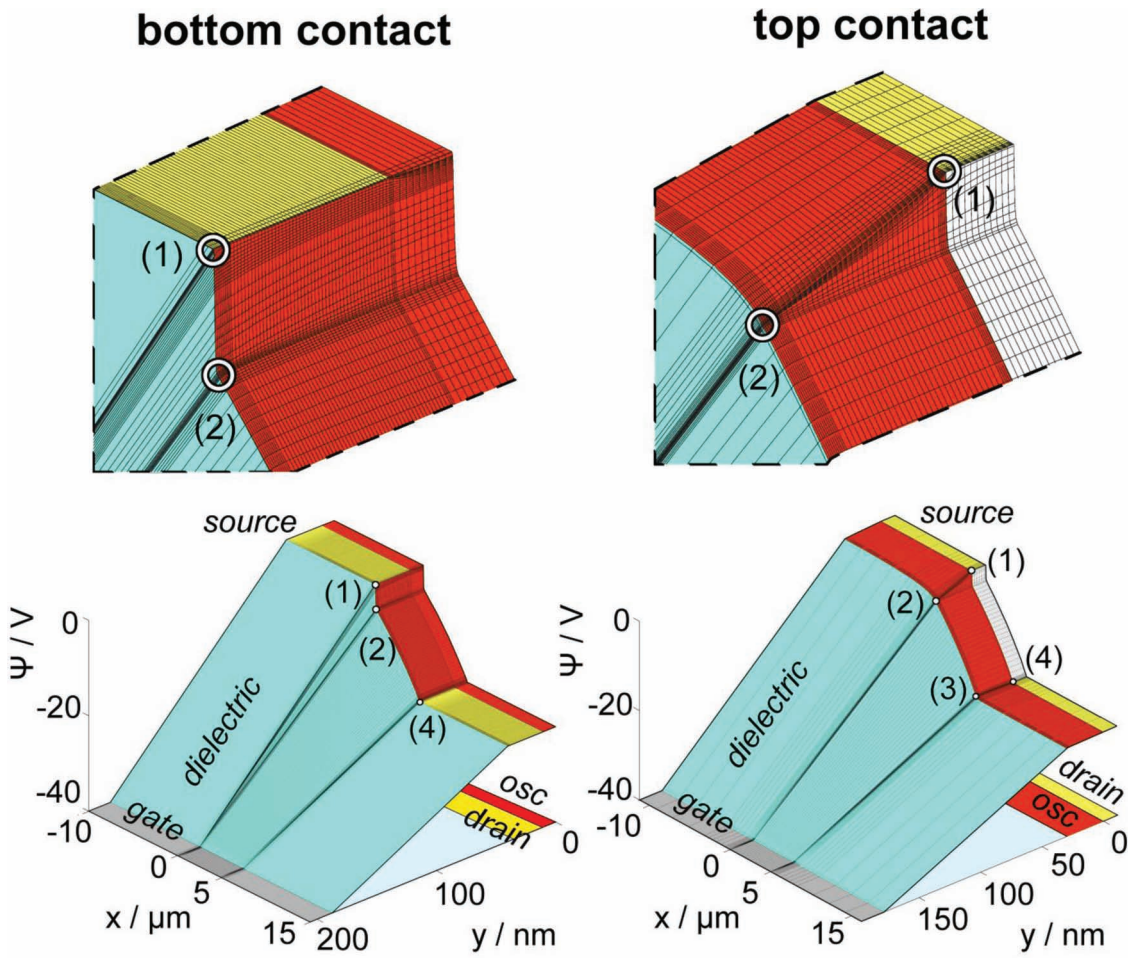

Figure 3. Steady state electrostatic potential for a BC (left panels) and a TC OTFT (right panels) across the entire device assuming a hole injection barrier $\Phi = 0.5$ eV and a mobility of $\mu = 1$ cm^2 V^{-1} s^{-1}. The transistor is operated at $V_{DS} = -20$ V and $V_{GS} = -40$ V. The top-panels show a zoom into the region around the source contacts.

clearly below 40% for the top-contact structure (green circles), it rises to more than 90% in the bottom-contact case at $\Phi = 0.8$ eV (black squares). The primary reason for the at the first glance surprising observation that the absolute change of R_C with Φ (Figure 2a) is significantly more pronounced than the change of R_C / R_{tot} (Figure 2c) is that due to the increased voltage drop at the contact at large R_C the channel potential is shifted only by part of the applied V_{GS}. This results in a reduced accumulation of charge carriers and, thus, also in an increased channel resistance.

To understand the extreme geometry dependence of the relation between Φ and R_C, it is instructive to first examine the typical electrostatic potential distribution in a device, which is the result of the applied bias voltages and of the build-up of a steady state concentration of carriers within the organic semiconductor. Of particular relevance in this context are the carriers in the immediate vicinity of the source contact. They change the local potential landscape and especially the barrier shaping field $E_\perp$ and, thus, also the effective barrier height Φ^*. Beyond that, in order to obtain a current through the OTFT, carriers must not only be injected at the metal-semiconductor interface but also need be collected from anywhere at the contact interface and funneled to the channel entrance (position (2) in Figure 1a,b). This happens through a carrier-collecting, continuous potential drop. In turn, both $E_\perp$ and Φ^* become dependent on the position at the contact interface[31] and the shape of the potential in the region of the source contact plays a crucial role.

The steady-state situations for BC and TC device cross-sections are shown in **Figures 3** together with zooms into the immediate source contact regions for a representative nominal injection barrier of $\Phi = 0.5$ eV. It is clearly seen that the variation of the potential in the region near the injecting source contact edge (1) and in the region near channel entrance (2) is strongly different between BC and TC devices. While there is a steep potential drop from (1) towards (2) in the BC geometry, the potential drop between (1) and (2) is much more gradual for the TC device. From the data shown in Figure 3 it can also be inferred that in the case of a BC device, the contact facet oriented parallel to the dielectric-semiconductor interface does not participate effectively in the injection due to a very small potential gradient that would transfer the injected carriers to

© 2013 WILEY-VCH Verlag GmbH & Co. KGaA, Weinheim

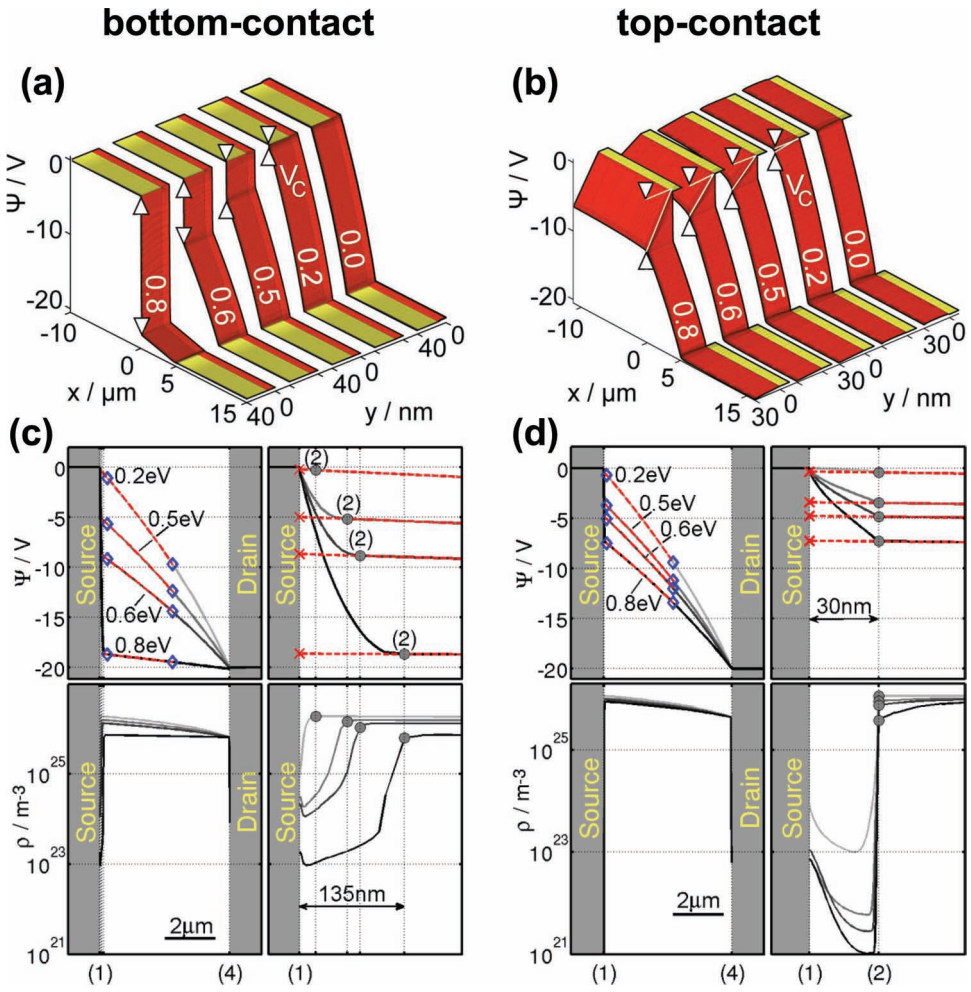

Figure 4. a,b) Steady state electrostatic potential in the organic semiconductor for BC (a) and TC type OTFTs (b) for several values of the nominal hole injection barrier Φ (varied between 0.0 eV and 0.8 eV) and for a mobility of $\mu = 1$ cm^2 V^{-1} s^{-1}. The transistors are operated at $V_{DS} = -20$ V and $V_{GS} = -40$ V. White arrows indicate the potential difference V_C between (1) and (2). c,d) Top left panels: Potential along the current pathway from the contact edge (1) via the channel entrance (2) to the end of the channel (4) for different values of Φ (0.2, 0.5, 0.6, and 0.8 eV) for BC (c) and TC OTFTs (d). Diamonds represent the regions where the potential is fitted (red dashed line) for the determination of V_C (for further details see Methods Section). Top right panels: Close up view on the potential between (1) and the channel entrance (2). The transition from a contact-related to the channel-related potential is marked with a circle; x mark the voltages that determine V_C obtained by extrapolating the fits to the metal-semiconductor interface (see Methods Section). Bottom panels: corresponding carrier densities in the organic semiconductor.

the channel. In contrast, in the top-contact transistor a potential gradient develops at the semiconductor-dielectric interface that collects also charges injected further away from the channel entrance. Which part of a top-contact is effectively injecting charges depends strongly on the magnitude of the injection barrier as described in detail in[31] and discussed briefly below.

For analyzing injection, it is useful to discriminate between different injection regimes, which have been proposed previously for top-contact transistors[31] and which can be equally well used to classify injection in bottom-contact setups. Depending on the nominal injection barrier height Φ, one can distinguish between quasi-ohmic (Q-O), barrier-regulated (B-R), and tunneling-injection (T-I). The ranges of barriers these regimes are associated with are indicated in Figure 2b with different shadings; they approximately correspond to the three regimes of $R_{C,TC}/R_{C,BC}$ ratios discussed above.

For understanding the Φ-dependence of the injection it is useful to consider the potentials within the semiconductor for different barrier heights. These are plotted in **Figure 4**, where also the Φ-dependent potential drop at the contact, V_C, is indicated. The corresponding evolutions of the potential along the current pathway from the contact edge (1) via the channel entrance (2) to the end of the channel (3) are shown in Figure 4c,d together with the associated charge distributions.

4.1.1. Small Injection-Barriers: Quasi-Ohmic Injection

For small injection barriers including $\Phi = 0$, quasi-ohmic injection occurs, i.e., the injected current exactly matches $I_{SD,\mu}$, the source-drain current determined by the bulk-limited current density, $j_{SD,\mu}$. The latter can be introduced in analogy to the quantity Shen et al. used for describing organic diodes.[49] It

© 2013 WILEY-VCH Verlag GmbH & Co. KGaA, Weinheim

corresponds to the current density the semiconductor sustains due to the local fields, the local equilibrium charge carrier concentration, and the material's mobility. When more carriers are injected locally than can be transported away due to $j_{SD,\mu}$, this results in the formation of a space-charge layer that drives further excess carriers back to the contact.[31] Such a situation is, for example, observed for the top-facet of the bottom contact, where due to the above-mentioned lack of a field transporting carriers to the channel-entrance a small potential hump (barely visible on the potential scale chosen for plotting Figure 4) is formed that drives carriers back into the contact.[50]

As for small barriers, the injected current density easily matches $j_{SD,\mu}$, the contact resistance there is primarily related to an access resistance, where V_C needs to ensure that the carriers located at position (1) (or anywhere else in the immediate vicinity of the contact) are transferred to the channel entrance (2). In top-contact devices this means that carriers need to be transported from the contact interface to the opposing dielectric-semiconductor interface and (if necessary) from there to the channel entrance. Between (1) and (2) V_C, thus, drops across a fixed access distance d_c that coincides with the thickness of the semiconductor d_{osc}, as can be seen in the close-up of the potential shown in the right panel of Figure 3. The magnitude of the potential drop necessary to maintain $I_{SD,\mu}$ depends not only on d_{osc}, but also on the area of the contact that injects charges[31] as well as on the (strongly reduced) carrier density between contact and channel (see lower panel in Figure 4d).

In the case of bottom-contact devices, the contact interface is already next to the dielectric-semiconductor interface. Thus, the associated access distance d_c is not fixed by the electrode or layer setup but depends on Φ (as can been seen in the right panels of Figure 4c). For $\Phi = 0.0$ eV and $\Phi = 0.2$ eV it is smaller than in the TC case. Moreover, for very small Φ there is no pronounced decrease in the carrier density between (1) and (2). For $\Phi = 0.0$ eV there is even an increase. (see Supporting Information). Both effects reduce R_C for the BC structure compared to the TC situation.

4.1.2. Intermediate Injection-Barriers: Barrier-Regulated Injection

Around $\Phi \approx 0.3$ eV (see Figure 2), quasi-ohmic injection is replaced by barrier-regulated injection. In this situation, the nominal injection barrier Φ would be too large to permit an injection current that is sufficiently large to sustain $I_{SD,\mu}$. As a consequence, V_C at the contact is increased to establish a barrier-shaping field $E_\perp$ that lowers the actual injection barrier Φ^* and, therefore, increases the injected current density.[17,31] The increase in V_C automatically reduces the potential drop over the channel and in turn reduces $I_{SD,\mu}$ (as the field driving carriers along the channel is reduced). In a first approximation, the combination of these two effects results in the injected current again matching the reduced $I_{SD,\mu}$. A closer inspection of the situation for BC and TC devices, however, reveals that there are additional mechanisms at work that are fundamentally different for the two device geometries:

In the case of TC devices, one finds that the active contact area participating in injection increases with increasing Φ,[17,31] i.e., starting from a few nanometers of active injection length in the quasi-ohmic regime (current crowding), the extension of the injection area parallel to the channel stretches across several micrometers for barriers of $\Phi = 0.5$ eV.[31] This area-enlargement facilitated injection effectively reduces V_C, and, consequently, results in a decrease of the contact resistance compared to a situation with injection form a fixed area. The occurrence of an analogous mechanism is prevented in the BC geometry, since the extension of the actively injecting contact area is limited by the height of the contact to a few ten nm. Moreover, the establishment of the barrier-regulating field $E_\perp$ is affected by a profound increase of d_c with Φ shown in the right panel in Figure 4c). While for $\Phi = 0.2$ eV, d_c only amounts to 20 nm, it rises to 66 nm at $\Phi = 0.3$ eV and, eventually, to 87 nm at $\Phi = 0.5$ eV. That is, beyond a certain injection barrier, the injection distance in BC devices exceeds that in their TC counterparts. The increase in d_c in the BC devices is accompanied by a strongly reduced carrier density (see Figure 4c). All these effects result in a deteriorating performance of the BC transistors compared to their TC counterparts with increasing Φ.

Finally, it should be noted that at small and intermediate barriers thermionic injection dominates over tunneling, as can be seen from a comparison of the corresponding contact resistances $R_{C,th}$ and $R_{C,tu}$ in Figure 2a. Note that these two quantities are defined such that $1/R_C = 1/R_{C,th} + 1/R_{C,tu}$ and $R_{C,th}/R_{C,tu} = I_{tu}/I_{th}$ (i.e., the net injected currents are corrected by I_{bf}).

4.1.3. High Injection-Barriers: Tunneling Injection

Upon further increasing Φ, $R_{C,th}$ continues rising faster with Φ for the BC than for the TC geometry. Moreover, beyond $\Phi \approx 0.5$ eV the contribution by tunneling injection becomes significant (up and down triangles in Figure 2a). The reason for that is that V_C must be increased so that $I_{SD,\mu}$ is provided by the contact also for large barriers. This increases the barrier shaping field, which narrows the barrier such that overcoming it by tunneling becomes more likely than by thermal activation.

In the case of TC transistors, $E_\perp$ is particularly large at the sharp edges of the source contact. This leads to an almost abrupt return to current crowding, since injection is again entirely accomplished within a few nm of position (1).[31] Nevertheless, the field enhancement as a result of the contact geometry is large enough that the tunneling-derived contribution to the contact resistance, $R_{C,tu}$, increases by only a factor of 1.3 between $\Phi = 0.6$ eV and $\Phi = 0.8$ eV. The situation is different for the BC geometry, as there increasing Φ also increases d_c. This limits the increase of $E_\perp$ and, thus, strongly reduces the tunneling current. Therefore, $R_{C,tu}$ keeps rising sharply with Φ in the BC transistor (by a factor of 17 between $\Phi = 0.6$ eV and $\Phi = 0.8$ eV).

4.1.4. Role of Barrier-Lowering

In the light of the comparison detailed above, the question arises for which of the two device architectures, the injection is more affected by the barrier-shaping field. Calculations we performed without considering the image-force term (2nd term in Equation (1)) for the devices discussed in Figure 2 indicate that the injection into BC transistors benefits more from the barrier-lowering effects than in the case TC devices, in accord with the findings of Brondijk et al.[29] This is, in part, a consequence

© 2013 WILEY-VCH Verlag GmbH & Co. KGaA, Weinheim

of the possibility of TC structures to enlarge the injecting area (vide supra). As a net effect, under operation conditions like those described in Figure 2, in the absence of the image-force term the injection into the BC device is almost totally suppressed, i.e., R_C/R_{tot} = 0.99, at Φ = 0.4 eV, while TC devices exhibit a non-negligible injection up to Φ = 0.7 eV.

4.2. Impact of the Point of Operation

4.2.1. Output Characteristics for BC and TC Devices

Having discussed the essential processes associated with injection at different barrier heights, we now turn to the description of the entire output characteristics $I_{SD}(V_{DS})$ as a function of Φ. These are contained in **Figure 5**a,b.The observed trends are similar for both contact alignments: i) with increasing Φ there is a continuous drop in the saturation current; ii) in the linear regime at small Φ, I_{SD} is strictly proportional to V_{DS}; iii) in contrast, at larger Φ the $I_{SD}(V_{DS})$ curve exhibits a pronounced lag, an effect often seen also in experiments for contact-limited transistors.[13,21,22,46,51] In passing we note that the observation of this non-linearity of $I_{SD}(V_{DS})$ for a constant hole mobility is at variance with previous reports,[24,32] where it has been suggested to be a consequence of the field-dependence of μ. Our findings, thus, support the claim by Brondijk et al.[29] that already the proper inclusion of mirror charge effects is sufficient for recovering that behavior.

In spite of the similar trends for TC and BC devices, the quantitative details of the evolution of the source-drain current with Φ and V_{DS} are different for the two device types: The above-described non-linearity at large Φ is more pronounced for BC devices and there the currents at large Φ are smaller both in the linear as well as in the saturation regime. This can be rationalized by the observation that in BC devices a much larger fraction of the total resistance arises from R_C (see Figure 5c,d). This reduces I_{SD} in two ways: A significant fraction of the applied V_{DS} drops over the contact reducing the driving voltage for current to flow through the channel. Moreover, the voltage drop over the contact reduces the shift of the channel potential induced by V_{GS}, which in turn reduces the conductivity of the channel.

In contrast to the poor performance of BC transistors at large Φ, at small barriers they outperform their TC counterparts. This happens not only deeply in the linear regime (as discussed already in the preceding section), but over the entire considered range of V_{DS} values. This is best seen in Figure 5e, where the ratio of the contact resistances for BC and TC devices is shown and where one also sees that the region of injection barriers at which $R_{C,BC}$ is smaller than $R_{C,TC}$ is even somewhat extended in the saturation regime. This can be rationalized by the larger barrier-shaping field in the vicinity of source contact at large V_{DS} that promotes carrier injection for BC devices more than for TC transistors.[29]

4.2.3. Transfer Characteristics for BC and TC Devices

The general trends observed for varying V_{GS} are reminiscent of those observed when changing V_{DS} (see Figure 5f,g): In both types of devices, large injection barriers result in the need for applying a significant bias in order to achieve current flow between source and drain with the effect again being more pronounced for bottom-contact devices (see Section 4.1.3). As a consequence, the maximum source-drain currents in the considered voltage range are significantly smaller for the BC devices in the high-Φ region.[29]

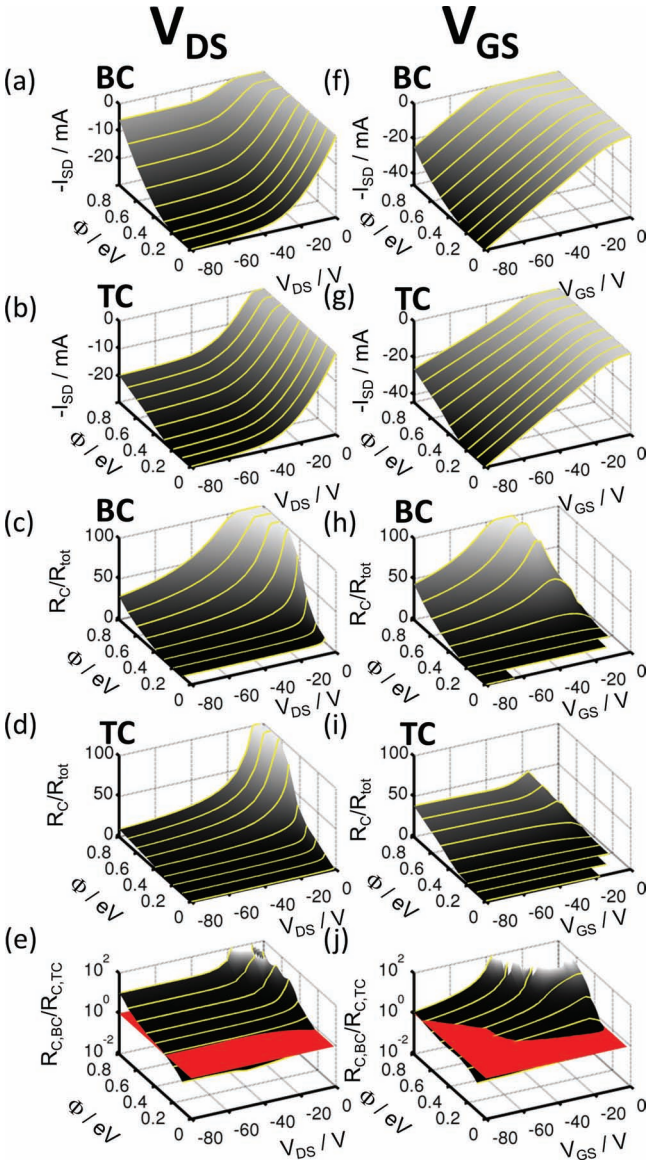

Figure 5. Impact of the contact resistance on the electrical characteristics of OTFTs. a,b) Output characteristics of BC and TC devices as a function of Φ. c,d) R_C/R_{tot} for BC and TC devices. In (e) the ratios between the contact resistances in BC and TC transistors as a function of Φ and V_{DS} are shown; the intersection with the red plane marks the V_{DS} values at which $R_{C,BC} = R_{C,TC}$. f–j) Equivalent plots for varying the gate-source instead of the drain-source voltage. The dimensions of the device are described in the main text; when varying V_{DS}, V_{GS} is set to –40 V and when varying V_{GS}, V_{DS} is set to –20 V. For BC no data for the contact resistances for Φ = 0 eV can be provided (see Methods Section).

© 2013 WILEY-VCH Verlag GmbH & Co. KGaA, Weinheim

The reason for the above-described "apparent shift" of the threshold voltage[52] is that at large barriers a significant field is required in the vicinity of the contact to enable the injection of a sufficiently large number of charge carriers with the effect being larger for BC devices as explained in section 4.1.3. Only the fraction of V_{GS} on top of that voltage drop eventually shifts the channel potential resulting in an accumulation of carriers.

Regarding the contribution of the contact resistance to the total resistance a pronounced maximum of R_C/R_{tot} is found (see Figure 5h,i). As V_C increases with decreasing $|V_{GS}|$ due to the lessened ability of the gate bias to lower the injection barrier, $R_C/R_{tot} = V_C/|V_{DS}|$ rises continuously. Due to the large aspect ratio, V_C, however, cannot exceed $|V_{GS}|$. Thus, R_C/R_{tot} has to be smaller than or at the most equal to $|V_{GS}|/|V_{DS}|$. As a consequence, when $|V_{GS}| << |V_{DS}|$ the relative contribution of R_C needs to decrease. As with increasing Φ the ratio R_C/R_{tot} rises more steeply with $|V_{GS}|$, the voltage at which the relative contribution of R_C reaches its maximum shifts to higher gate biases.

When analyzing the relative impact of the contact resistance for top- and bottom-contact devices as a function of Φ and V_{GS} again several relevant observations can be made (see Figure 5j): For small barriers, the contact resistance is always smaller for BC devices irrespective of the applied gate voltage (see Section 4.1.1). The barrier Φ for which the contact resistances of the two device structures are identical, however, shifts to significantly higher barriers, when increasing $|V_{GS}|$.[29] The pronounced kink in the $R_{C,BC} = R_{C,TC}$ curve at $|V_{GS}| \approx 55$ V marks the cross-over from thermionic barrier-regulated to tunneling injection. The $|V_{GS}|$ values necessary to achieve the same $R_{C,tu}$ due to tunneling ($|V_{GS}| > 55$ V) differ much more between BC and TC geometry than those $|V_{GS}|$ required for the same $R_{C,th}$ ($|V_{GS}| < 55$ V). Moreover, the penalty one has to pay for using a BC device geometry becomes exceedingly large at small $|V_{GS}|$ when Φ exceeds ≈0.3 eV (i.e., when the barrier-shaping field due to V_{GS} [52] becomes small compared to the barrier height Φ).

5. Role of the Charge-Carrier Mobility for the Contact Resistance

Finally, it shall be discussed to what extent the above conclusions are impacted by the mobility of the used semiconductor material. To that aim, we plot in **Figure 6** as open symbols the ratio between the contact resistance and the total resistance of the transistor, R_C/R_{tot}, as a function of μ for three injection barriers. As R_C/R_{tot} per definition equals V_C/V_{DS}, such a plot has the advantage of directly revealing, how much of the applied V_{DS} (in our case –20 V) drops at the contact. Also the absolute values of $R_C(\mu)$ are shown (as filled symbols).

The main trends discussed in Section 4 for $\mu = 1$ cm^2 V^{-1} s^{-1} (grey bar in Figure 6) are preserved also for all other μ-values: At small Φ, R_C is clearly smaller in the BC than in the TC geometry, for Φ around 0.5 eV the two geometries perform very similarly, and at large barriers ($\Phi = 0.7$ eV), the top-contact geometry is superior. Regarding the injection mechanism, the generally observed trend is that at small barriers thermionic injection dominates, while the contribution of tunneling injection increases with Φ in particular at large μ. The corresponding

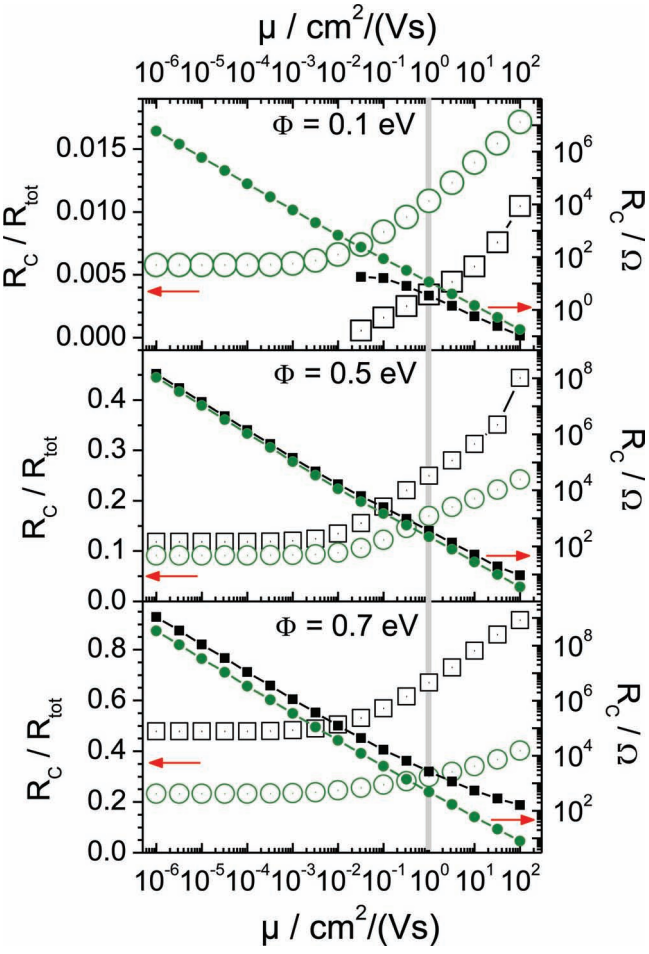

Figure 6. Open symbols: ratio of the contact resistance, R_C, and the total resistance R_{tot} in bottom-contact (black squares) and top-contact (green circles) OTFTs as a function of the hole mobility, μ, for different Φ (top plot: $\Phi = 0.1$ eV; central plot: $\Phi = 0.5$ eV; bottom plot: $\Phi = 0.7$ eV). Filled symbols: absolute values of the corresponding contact resistances. V_{DS} has been set to –20 V and V_{GS} to –40 V. The fact that $V_C/V_{DS} = R_C/R_{tot}$ results in V_C (in V) = $-20R_C/R_{tot}$. For BC devices, no data for the contact resistances for mobilities $\mu \leq 0.01$ cm^2 V^{-1} s^{-1} and for $\Phi = 0.1$ eV can be provided (as explained in the Methods Section).

plots analyzing the contributions of R_{th} and R_{tu} can be found in the Supporting Information. Why large barriers favor tunneling injection is discussed in Section 4.1.3; the observation that tunneling also dominates at large μ is ascribed to the fact that the resulting large bulk-limited current densities give rise to a comparably larger potential drop at the contact (see Figure 6) and, consequently, also a reduced tunneling barrier especially for top-contact devices (see Figure 4d), where the injection length, d_c, is not impacted by V_C.

Another interesting finding is that for all barriers R_C/R_{tot} is hardly affected by μ as long as the mobilities are not too large. As R_{tot} strongly decreases with increasing μ, this means that the same applies to R_C. In fact we find that the channel resistance R_{ch} is proportional to $1/\mu$ for all three investigated barriers and contact geometries (linear fits see Supporting Information), which means that also R_C is proportional to $1/\mu$

© 2013 WILEY-VCH Verlag GmbH & Co. KGaA, Weinheim

up to $\mu \approx 10^{-2}$ cm^2 V^{-1} s^{-1}.[54] This strong μ-dependence of R_C can be explained by associating it with an access resistance. For small μ, more than enough carriers can overcome the injection barrier to maintain $I_{SD,\mu}$, but they do not necessarily reach the channel entrance. This is because they first have to cross the "access" region depleted of carriers (see Figure 4c), whose resistivity is proportional to $1/\mu$.[55] V_C remains essentially constant at small μ (following from it being proportional to R_C/R_{tot}, vide supra), which results in a μ-independent access distance d_c also for bottom contact devices. As a consequence, R_C becomes proportional to $1/\mu$ for BC and, provided that the injecting area does not change significantly with μ, also for TC devices. The assumption that for small μ the main source of the contact resistance is the difficulty for carriers to reach the channel is fully consistent with our observation that then the back-flowing current, I_{bf}, nearly entirely compensates the injected one independent of device geometry and Φ. This behavior is exemplarily shown for TC devices at $\Phi = 0.1$ eV in Figure 1d. The strong increase of R_C/R_{tot} with the injection barrier can for the low-μ regime be rationalized by the observation that the degree to which the access region is depleted of carriers (i.e., its conductivity) strongly depends on the injection barrier (see Figure 4c).

For larger μ and, thus, increasing $I_{SD,\mu}$, the voltage drop at the contact (and, consequently, R_C/R_{tot}) has to increase to provide a sufficiently large barrier-shaping field such that the effective barrier, Φ^*, is reduced enough to allow the injection of a sufficient number of carriers (as discussed for $\mu = 1$ cm^2 V^{-1} s^{-1} in Section 4.1.2). Figure 6 appears to suggest that this happens as a sharp transition at a specific mobility that is not affected very much by Φ. This impression is, however, primarily a consequence of the logarithmic μ-scale chosen for the plot to better visualize the situation at small μ. This becomes obvious from choosing a linear mobility scale, as is done in the Supporting Information.

6. Conclusions

From what is said above it can be concluded that the injection-barrier between the electrode Fermi-level and the transport-level in the semiconductor is only one of many parameters determining the contact resistance at the source-electrode of an organic transistor. Also the value of the mobility of the used organic semiconductor can change R_C by many orders of magnitude. The contact resistance also profoundly decreases with increasing gate-source and drain-source voltages. Moreover, the choice of the device geometry (bottom- vs. top-contact) has a significant impact on the device performance. In contrast to several claims in the literature we do not find for idealized devices (assuming flat interfaces, a constant μ and disregarding traps) that top-contact devices necessarily outperform their bottom-contact counterparts. It is rather shown that at small barriers, the contact resistance for BC devices is smaller than in their TC counterparts irrespective of the semiconductor mobility and the point of operation. This can be explained by the specific field and carrier-density distributions within the device. In fact, the ratio between $R_{C,TC}$ and $R_{C,BC}$ changes by several orders of magnitude for otherwise identical device properties, when changing Φ or the operation conditions. Generally, we find that BC devices outperform their TC counterparts for small injection barriers (Figure 2, 5, and 6), high gate-source voltages (Figure 5), and low mobilities (Figure 6). On more technical grounds it is clearly shown that for obtaining a comprehensive picture of the intrinsic contact resistance, all currents at the interface (thermionic, tunneling, and back-flowing) and in accord with[29] also all barrier shaping fields need to be considered. The above results highlight the crucial need for a tight integration of materials investigations (to determine, e.g., μ and Φ) and the consideration of device aspects (such as the device geometry).

7. Methods Section

Charge Transport: The drift-diffusion model was employed here as is commonly done for organic devices (see, e.g., ref. [5,17,24]). The transport of a charge carrier was assumed to take place in a single transport level (δ-shaped density of states) with an effective hole mass set equal to the electron mass m_e; all effects due to a finite band width and/or due to disorder could be accounted for by choosing a field- and concentration-dependent mobility, which was, however, not done here, as the interest was in general trends (see discussion in the Introduction).

Determination of the Barrier-Shaping Field $E_\perp$: According to the injection model used (Section 2.1), an $r_\perp$-independent electric field $E_\perp$ was assumed in the vicinity of the source contact to obtain the current densities j_{th} and j_{tu}. The actual electric field, $E_{\perp,PE}(r_\perp)$, as obtained from the Poisson equation, was, however, not exactly constant in that region; the absolute value of $|E_{\perp,PE}|$ was largest at $r_\perp = 0$ and dropped with increasing distance from the contact. Rather than simply assigning the value of $E_{\perp,PE}$ at $r_\perp = 0$ to the model field $E_\perp$ (leading to an overestimation of $E_\perp$), the following approximation was used: based on the self-consistently obtained electro-static potential distribution, $\Psi(r)$, the distance from the contact interface at which $\Psi(r)$ equals the chemical potential of the metal was determined (see Figure 1c); combining this distance with the associated potential drop (that, by definition, equaled Φ in Figure 1c) an approximate constant $E_\perp$ was obtained.[31]

Determination of the Contact Voltage V_C : For obtaining V_C in BC devices, the potential in the channel region was fitted (details are given in the Supporting Information) at the semiconductor-dielectric interface by a cubic polynomial. This fit was then extrapolated to position (1) (dashed lines in Figure 4c). The difference between the extrapolated channel potential at (1) (red crosses in Figure 4c) and the actual source potential is then taken as V_C in this way associating only the potential modification due to the contact with R_C. The distance between the end of the source contact and the position where the deviation of the true potential from the fit becames smaller than a certain value (here set to 0.01 V) was interpreted as the injection distance.

Note, that for BC devices, the exact position of (2) strongly depended on the injection barrier, device dimensions and operating point and was, therefore, not stationary.

For the sake of consistency, the same procedure was applied to the TC transistors for determining V_C; d_c, however, does not change and is given by the thickness of the semiconductor layer. The contact resistance determined in this way was slightly reduced compared to that determined when associating V_C with

© 2013 WILEY-VCH Verlag GmbH & Co. KGaA, Weinheim

the difference between the potential at the source contact and the potential at (2), but this did not affect the discussed trends.

Note that this definition of R_C led to ill-defined values of the contact resistance in BC devices for small Φ in combination with low mobilities, as in such cases a space-charge layer forms close to the contact. This then gave rise to a potential hump, for which the above described extrapolation of the fit yielded a negative V_C, which, in turn, resulted in a negative R_C. This was the reason why it was not possible to report values for the contact resistances of BC devices for $\mu = 1$ cm^2 V^{-1} s^{-1} and $\Phi =$ 0 eV in Figure 2 and for $\mu \leq 0.01$ cm^2 V^{-1} s^{-1}and $\Phi = 0.1$ eV in Figure 6. Moreover, for large Φ at small $|V_{GS}|$ vanishingly small currents prevented a reliable calculation of R_C.

Determination of Contact Resistance Contributions: The contact resistances due to thermionic emission and due to tunneling were defined as $R_{C,th} = V_C/(pI_{th})$ and $R_{C,tu} = V_C/(pI_{tu})$; here, the partition factor $p = 1\text{-}I_{bf}/(I_{th}+I_{tu})$ was chosen such that the contributions of the back-flowing current to a net thermionic and a net tunneling injection current were proportional to I_{th} and I_{tu}, respectively.[31]

Supporting Information

Supporting Information is available from the Wiley Online Library or from the author.

Acknowledgements

This work has been supported by the Austrian Nanoinitiative (FFG) through the NILsimtos project as part of the NILaustria cluster.

Received: November 5, 2012
Revised: December 4, 2012
Published online: January 23, 2013

[1] J. Z. Wang, Z. H. Zheng, H. Sirringhaus, *Appl. Phys. Lett.* **2006**, *89*, 083513.
[2] U. Haas, H. Gold, A. Haase, G. Jakopic, B. Stadlober, *Appl. Phys. Lett.* **2007**, *91*, 043511.
[3] B. Stadlober, U. Haas, H. Gold, A. Haase, G. Jakopic, G. Leising, N. Koch, S. Rentenberger, E. Zojer, *Adv. Funct. Mater.* **2007**, *17*, 2687.
[4] T. J. Richards, H. Sirringhaus , *J. Appl. Phys.* **2007**,*102*, 094510.
[5] S. K. Possanner, K. Zojer, P. Pacher, E. Zojer, F. Schürrer, *Adv. Funct. Mater.* **2009**, *19*, 958.
[6] M. F. Calhoun, J. Sanchez, D. Olaya, M. E. Gershenson, V. Podzorov, *Nat. Mater.* **2008**, *7*, 84.
[7] F. Ante, D. Kälblein, U. Zschieschang, T. Canzler, A. Werner, K. Takimiya, M. Ikeda, T. Sekitani, T. Someya, H. Klauk, *Small* **2011**, *7*, 1186.
[8] P. V. Pesavento, K. P. Puntambekar, C. D. Frisbie, J. C. McKeen, P. P. Ruden, *J. Appl. Phys.* **2006**, *99*, 094504.
[9] B. H. Hamadani, D. Natelson, *Proc. IEEE* **2005**, *93*, 1306.
[10] A. S. Molinari, H. Alves, Z. Chen, A. Facchetti, A. F. Morpurgo, *J. Am. Chem. Soc.* **2009**, *131*, 2462.
[11] C. Reese, Z. Bao, *Mater. Today* **2007**, *10*, 20.
[12] O. Acton, M. Dubey, T. Weidner, K. M. O Malley, T.-W. Kim, G. G. Ting, D. Hutchins, J. E. Baio, T. C. Lovejoy, A. H. Gage, D. G. Castner, H. Ma, A. K.-Y. Jen, *Adv. Funct. Mater.* **2011**, *21*, 1476.
[13] N. Kawasaki, Y. Ohta, Y. Kubozono, A. Fujiwara, *Appl. Phys. Lett.* **2007**, *91*, 123518.
[14] a) T. Minari, T. Miyadera, K. Tsukagoshi, Y. Aoyagi, H. Ito, *Appl. Phys. Lett.* **2007**, *91*, 053508; b) C. Vanoni, S. Tsujino, T. A. Jung, *Appl. Phys. Lett.* **2007**, *90*, 193119; c) C. Vanoni, T. A. Jung, S. Tsujino, *Appl. Phys. Lett.* **2009**, *94*, 253306.
[15] M. Kano, T. Minari, K. Tsukagoshi, *Appl. Phys. Lett.* **2009**, *94*, 143304.
[16] Y. Zhou, C. Fuentes-Hernandez, J. Shim, J. Meyer, A. J. Giordano, H. Li, P. Winget, T. Papadopoulos, H. Cheun, J. Kim, M. Fenoll, A. Dindar, W. Haske, E. Najafabadi, T. M. Khan, H. Sojoudi, S. Barlow, S. Graham, J.-L. Brédas, S. R. Marder, A. Kahn, B. Kippelen, *Science* **2012**, *336*, 327.
[17] N. Tessler, Y. Roichman, *Appl. Phys. Lett.* **2001**, *79*, 2987.
[18] S. D. Wang, T. Minari, T. Miyadera, K. Tsukagoshi, Y. Aoyagi, *Appl. Phys. Lett.* **2007**, *91*, 203508.
[19] P. Necliudov, M. Shur, D. Gundlach, T. Jackson, *Solid-State Electron.* **2003**, *47*, 259.
[20] I. G. Hill, *Appl. Phys. Lett.* **2005**, *87*, 163505.
[21] D. J. Gundlach, L. Zhou, J. A. Nichols, T. N. Jackson, P. V. Necliudov, M. S. Shur, *J. Appl. Phys.* **2006**, *100*, 024509.
[22] R. A. Street A. Salleo, *Appl. Phys. Lett.* **2002**, *81*, 2887.
[23] S. D. Wang, Y. Yan, K. Tsukagoshi, *Appl. Phys. Lett.* **2010**, *97*, 063307.
[24] S. Scheinert, G. Paasch, *J. Appl. Phys.* **2009**, *105*, 014509.
[25] P. V. Pesavento, R. J. Chesterfield, C. R. Newman, C. D. Frisbie, *J. Appl. Phys.* **2004**, *96*, 7312.
[26] D. Braga G. Horowitz, *Adv. Mater.* **2009**, *21*, 1473.
[27] a) M. J. Deen, M. H. Kazemeini, S. Holdcroft, *J. Appl. Phys.* **2008**, *103*, 124509; b) D. Gupta, M. Katiyar, D. Gupta, *Org. Electron.* **2009**, *10*, 775.
[28] V. Vinciguerra, M. L. Rosa, D. Nicolosi, G. Sicurella, L. Occhipinti, *Org. Electron.* **2009**, *10*, 1074.
[29] J. J. Brondijk, F. Torricelli, E. C. P. Smits, P. W. M. Blom, D. M. de Leeuw, *Org. Electron.* **2012**, *13*, 1526.
[30] S. J. Ausserlechner, M. Gruber, R. Hetzel, H.-G. Flesch, L. Ladinig, L. Hauser, A. Haase, M. Buchner, F. Schürrer, B. Stadlober, G. Trimmel, K. Zojer, E. Zojer, *Phys. Status Solidi A* **2012**, *209*, 181.
[31] M. Gruber, F. Schürrer, K. Zojer, *Org. Electron.* **2012**, *13*, 1887.
[32] A. Bolognesi, A. Di Carlo, P. Lugli, *Appl. Phys. Lett.* **2002**, *81*, 4646.
[33] a) J. Zaumseil, K. W. Baldwin, J. A. Rogers, *J. Appl. Phys.* **2003**, *93*, 6117; b) H. Klauk, G. Schmidt, W. Radlik, W. Weber, L. S. Zhou, C. D. Sheraw, J. A. Nichols, T. N. Jackson, *Solid-State Electron.* **2003**, *47*, 29; c) G. Horowitz, *J. Mater. Res.* **2004**, *19*, 1946; d) M. Kitamura, S. Aomori, J. H. Na, Y. Arakawa, *Appl. Phys. Lett.* **2008**, *93*, 033313.
[34] G. Horowitz, in *Organic Field-Effect Transistors* (Eds: Z. Bao, J. Locklin), Taylor & Francis, New York **2007**, Ch. 2.2.
[35] a) C. Y. Chang, S. M. Sze, *Solid-State Electron.* **1970**, *13*, 727; b) J. M. Shannon, *Solid-State Electron.* **1976**, *19*, 537.
[36] V. I. Arkhipov, U. Wolf, H. Bässler, *Phys. Rev. B* **1999**, *59*, 7514.
[37] P. S. Davids, I. H. Campell, D. L. Smith, *J. Appl. Phys.* **1997**, *82*, 6319.
[38] This is at least a very good approximation, as in the channel region the current flows within a few nanometers of the semiconductor/dielectric interface.
[39] Note that this is not to be confused with the pinch-off generated voltage drop at the drain that occurs, when operating devices in the saturation regime. This voltage drop is observed experimentally but has nothing to do with the contact.
[40] L. Bürgi, T. J. Richards, R. H. Friend, H. Sirringhaus, *J. Appl. Phys.* **2003**, *94*, 6129.
[41] Note that the specific choice of the value of the deviation between the true potential and the fit introduces some ambiguity regarding the determination of the exact position of (2); moreover the choice of the grid also has a minor impact. This prompted us not to take

© 2013 WILEY-VCH Verlag GmbH & Co. KGaA, Weinheim

the potential at (2) as the reference for the determination of V_C but rather use the value obtained in the extrapolation.
[42] F. Amy, C. Chan, A. Kahn, *Org. Electron.* **2005**, *6*, 85.
[43] N. J. Watkins, L. Yan, Y. Gao, *Appl. Phys. Lett.* **2002**, *80*, 4384.
[44] L. Diao, C. D. Frisbie, D. D. Schroepfer, P. P. Ruden, *J. Appl. Phys.* **2007**, *101*, 014510.
[45] N. Koch, A. Kahn, J. Ghijsen, J.-J. Pireaux, J. Schwartz, R. L. Johnson, A. Elschner, *Appl. Phys. Lett.* **2003**, *82*, 70.
[46] B. H. Hamadani D. Natelson, *J. Appl. Phys.* **2005**, *97*, 064508.
[47] E. J. Meijer, C. Tanase, P. Blom, E. van Veenendaal, B.-H. Huisman, D. M. de Leeuw, T. M. Klapwijk, *Appl. Phys. Lett.* **2002**, *80*, 3838.
[48] Note that we could not recover the R_C values given in ref. [20] even though we used the same device dimensions and material parameters. According to our analysis, this deviation originates, at least in part, from a very profound difference between the R_C values determined with our approach those deduced from the transfer-line method employed in ref. [20].
[49] Y. Shen, A. R. Hosseini, M. H. Wong, G. G. Malliaras, *ChemPhysChem* **2004**, *5*, 16.
[50] In fact, at very small barriers a few percent of the total current come from the top facet of the bottom contacts, which is a consequence of carrier diffusion that becomes relevant due to the enhanced carrier concentration above the contact.
[51] M. Kitamura, S. Aomori, J. H. Na, Y. Arakawa, *Appl. Phys. Lett.* **2008**, *93*, 033313.
[52] Note that this effect is not to be confused with the onset-voltage shift caused by a space-charge or dipole layer between the semiconductor and the dielectric (see ref. [5]). Here the resulting decrease of I_{SD} at small V_{GS} is much more gradual.
[53] Note that due to the large aspect ratio of OTFTs with channel lengths of typically several micrometers and dielectric thicknesses on the order of 100 nm, the barrier shaping field also for BC devices primarily originates from V_{GS} and not from V_{DS}.
[54] This is true also when the contribution of R_C to R_{tot} is no longer negligible, as even then R_C is directly proportional to R_{ch}.
[55] Indeed, we find a clearly linear relation between the channel resistance and $1/\mu$ in all investigated cases, which, in turn, results in R_C being directly proportional to $1/\mu$.

© 2013 WILEY-VCH Verlag GmbH & Co. KGaA, Weinheim